

Journal Pre-proof

Interrogating cadmium and lead biosorption mechanisms by *Simplicillium chinense* via infrared spectroscopy

Zhongmin Jin, Lin Xie, Tuo Zhang, Lijie Liu, Tom Black, Kevin C. Jones, Hao Zhang, Xinzi Wang, Naifu Jin, Dayi Zhang



PII: S0269-7491(20)30853-8

DOI: <https://doi.org/10.1016/j.envpol.2020.114419>

Reference: ENPO 114419

To appear in: *Environmental Pollution*

Received Date: 5 February 2020

Revised Date: 29 February 2020

Accepted Date: 18 March 2020

Please cite this article as: Jin, Z., Xie, L., Zhang, T., Liu, L., Black, T., Jones, K.C., Zhang, H., Wang, X., Jin, N., Zhang, D., Interrogating cadmium and lead biosorption mechanisms by *Simplicillium chinense* via infrared spectroscopy, *Environmental Pollution* (2020), doi: <https://doi.org/10.1016/j.envpol.2020.114419>.

This is a PDF file of an article that has undergone enhancements after acceptance, such as the addition of a cover page and metadata, and formatting for readability, but it is not yet the definitive version of record. This version will undergo additional copyediting, typesetting and review before it is published in its final form, but we are providing this version to give early visibility of the article. Please note that, during the production process, errors may be discovered which could affect the content, and all legal disclaimers that apply to the journal pertain.

© 2020 Published by Elsevier Ltd.

CRedit author statement

Zhongmin Jin: Investigation, Supervision, Writing- Original draft preparation. Lin Xie: Data curation, Visualization. Tuo Zhang: Investigation, Data curation. Lijie Liu: Data curation. Tom Black: Investigation, Data curation. Kevin C Jones: Resources, Data curation. Hao Zhang: Resources, Data curation. Xinzi Wang: Data curation, Visualization. Naifu Jin: Investigation, Data curation, Visualization, Writing- Original draft preparation. Dayi Zhang: Conceptualization, Methodology, Resources, Writing- Original draft preparation, Writing- Reviewing and Editing.

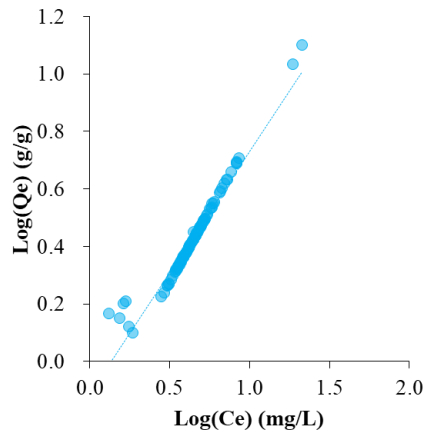
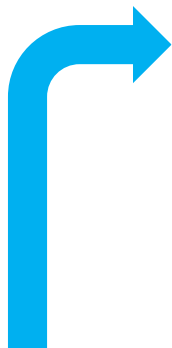


Simplicillium chinense

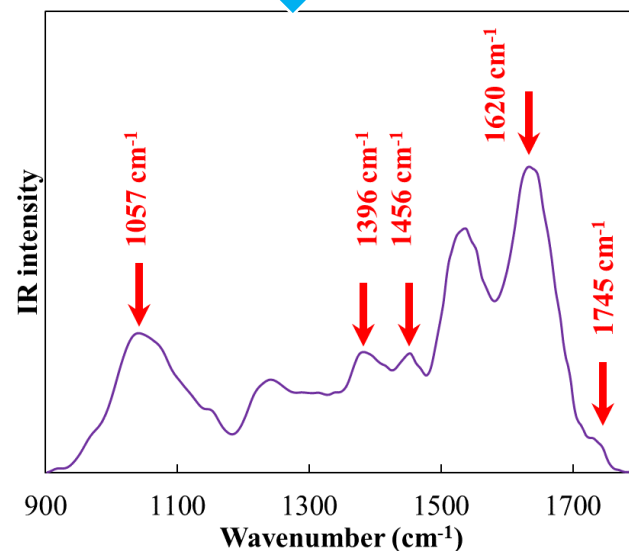


Cultivation with 48 carbons sources on PM4 plate

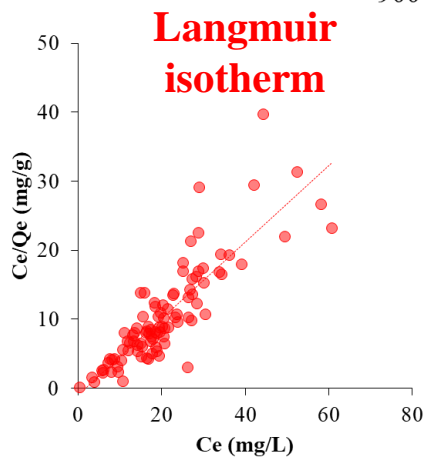
Pb biosorption



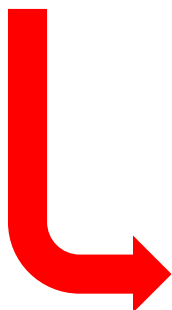
No biomarker for Pb biosorption



Five biomarkers for Pb biosorption



Cd biosorption



1 **Interrogating cadmium and lead biosorption mechanisms by**

2 ***Simplicillium chinense* via infrared spectroscopy**

3 Zhongmin Jin^{1,2}, Lin Xie¹, Tuo Zhang³, Lijie Liu¹, Tom Black², Kevin C Jones², Hao
4 Zhang², Xinzi Wang², Naifu Jin⁴, Dayi Zhang^{4,*}

5 1. College of Agriculture, Forestry and Life Science, Qiqihar University, Qiqihar
6 161006, PR China

7 2. Lancaster Environment Centre, Lancaster University, Lancaster LA1 4YQ, UK

8 3. College of Environmental Science and Engineering, China West Normal
9 University, Nanchong 637002, PR China

10 4. School of Environment, Tsinghua University, Beijing 100084, PR China

11

12 ***Corresponding author**

13 Dr Dayi Zhang

14 School of Environment, Tsinghua University, Beijing, 100084, PR China

15 Tel.: +86(0)1062773232; Fax: +86(0)1062785687

16 Email: zhangdayi@tsinghua.edu.cn

17

18 Abstract

19 Fungi-associated phytoremediation is an environmentally friendly and cost-efficient
20 approach to removal potential toxic elements (PTEs) from contaminated soils. Many
21 fungal strains have been reported to possess PTE-biosorption behaviour which
22 benefits phytoremediation performance. Nevertheless, most studies are limited in rich
23 or defined medium, far away from the real-world scenarios where nutrients are
24 deficient. Understanding fungal PTE-biosorption performance and influential factors
25 in soil environment can expand their application potential and is urgently needed. This
26 study applied attenuated total reflection Fourier-transform infrared (ATR-FTIR)
27 coupled with phenotypic microarrays to study the biospectral alterations of a fungal
28 strain *Simplicillium chinense* QD10 and explore the mechanisms of Cd and Pb
29 biosorption. Both Cd and Pb were efficiently adsorbed by *S. chinense* QD10
30 cultivated with 48 different carbon sources and the biosorption efficiency
31 achieved >90%. As the first study using spectroscopic tools to analyse
32 PTE-biosorption by fungal cells in a high-throughput manner, our results indicated
33 that spectral biomarkers associated with phosphor-lipids and proteins (1745 cm⁻¹,
34 1456 cm⁻¹ and 1396 cm⁻¹) were significantly correlated with Cd biosorption,
35 suggesting the cell wall components of *S. chinense* QD10 as the primary interactive
36 targets. In contrast, there was no any spectral biomarker associated with Pb
37 biosorption. Additionally, adsorption isotherms evidenced a Langmuir model for Cd
38 biosorption but a Freundlich model for Pb biosorption. Accordingly, Pb and Cd
39 biosorption by *S. chinense* QD10 followed discriminating mechanisms, specific
40 adsorption on cell membrane for Cd and unspecific extracellular precipitation for Pb.
41 This work lends new insights into the mechanisms of PTE-biosorption *via* IR
42 spectrochemical tools, which provide more comprehensive clues for biosorption

43 behaviour with a nondestructive and high-throughput manner solving the traditional
44 technical barrier regarding the real-world scenarios.

45 **Keywords:** cadmium, lead, biosorption, phytoremediation, carbon sources,
46 ATR-FTIR spectroscopy

47

Journal Pre-proof

48 1. Introduction

49 With the increasing development of many metal-related industries, *e.g.*, metal mining,
50 metal surface treating, energy production and fertilizer manufacturing, some metals
51 (mercury, chromium, etc.) or non-metals (arsenic, selenium, etc.) possessing potential
52 toxicities to human health are named as potential toxic elements (PTEs) and have
53 become one of the most critical sources of environmental contamination (Dong et al.,
54 2010). Industrial residues containing PTEs are continuously discharged into the
55 environment, posing vital threats to human life and ecosystems (Dong et al., 2010;
56 Liu et al., 2013). PTE-induced toxicity has been recognized to last for an extended
57 time in nature and accumulate in the food chain. The presence of PTEs even in traces
58 is harmful to both flora and fauna, cadmium (Cd) exposure for instance, which may
59 cause irreversible tubular damage in kidney (Järup, 2003; Leonard et al., 2004).
60 Numerous PTE-contaminated sites have been identified and require remediation
61 (Huang et al., 2019; Jiang et al., 2019).

62 To remediate PTE-contaminated soils and reduce the exposure possibility, several
63 approaches are developed and applied, including solidification (Tantawy et al., 2012),
64 elution (Rui et al., 2019), phytoremediation (Jiang et al., 2018; Jin et al., 2019).
65 Stabilization aims to adsorb or reduce PTEs, transferring unstable PTEs into stable
66 phases with less availability, *e.g.*, hydroxides and minerals (Wang and Vipulanandan,
67 2001; Yuan et al., 2018). Stabilizers include natural minerals (Gheju et al., 2016),
68 modified minerals (Ou et al., 2018; Sha et al., 2018; Singh et al., 2017), synthetic
69 materials (Liu et al., 2014; Sarkar et al., 2010), and reductive reagents (Geelhoed et al.,
70 2003; Patterson et al., 1997). However, the long-term stability of stabilization strategy
71 remains doubtful. Elution uses solvents to form PTE-chelates and enhance PTE
72 mobility (Khan et al., 2010), but suffers from the poor efficiency in clay-rich soils

73 owing to the relatively smaller osmotic coefficient which significantly abates PTE
74 mobility (Bolan et al., 2014; Rui et al., 2019). Biosorption which uses biomaterials
75 (bacteria, fungi, yeasts and plants) is highlighted as an alternative remediation
76 approach for PTEs (Wang and Chen, 2006). Comparing to other approaches,
77 biosorption is relatively cost-efficient, particularly for soils with low PTE levels (Yan
78 and Viraraghavan, 2003) or co-contaminated with other organic compounds (Deng et
79 al., 2018b). Phytoremediation is environmentally friendly to clean PTE-contaminated
80 soils and remain soil functions (Wiszniewska et al., 2016). Plants generally handle the
81 contaminants without damaging soil properties via an enormous ability to uptake and
82 detoxify PTEs by various mechanisms, such as uptake by roots, translocation to aerial
83 tissues and PTE- complexation with organic substances (Ali et al., 2013; Liu et al.,
84 2019).

85 In the soil ecosystem, the major soil biomass and biodiversity are formed by
86 microorganisms (Jin et al., 2019). Their presence in the rhizosphere plays important
87 roles in PTE phytoremediation (Jin et al., 2019; Khan, 2005). Cr phytoremediation,
88 for instance, is only effective for exchangeable or available Cr in soils (Shaheen et al.,
89 2019). Most phytoremediation practices use soil microbes or leaching reagents to
90 enhance PTE removal performance since their availability is strongly linked with soil
91 microbial activities (Deng et al., 2018a; Yin et al., 2015). Fungi, as one critical group
92 of microorganisms, have been applied as metal biosorbents in phytoremediation in
93 prior studies (Say et al., 2001). PTE biosorption capability of *Saccharomyces*
94 *Cerevisiae* ranges from 10 to 300 mg/g dry-cell-weight (DCW) for lead (Pb) and 10 to
95 100 mg/g DCW for Cd (Wang and Chen, 2006). *Penicillium* sp. MRF-1 has a strong
96 Cd biosorption capacity (0.13-9.39 mg/g DCW) (Velmurugan et al., 2010) and the
97 maximum biosorption capacity of *Exiguobacterium* sp. is 15.6 mg/g DCW for Cd

98 (Park and Chon, 2016). The mechanisms of fungal PTE biosorption are complicated
99 and mainly consist of two key stages: direct adsorption on fungal membrane and
100 penetration through cell wall. The first stage is a passive biosorption process
101 independent on fungal metabolism, and the key influential factor is the functional
102 groups on cell membrane which affect the interactions between fungal cells and PTE
103 ions (Leonard et al., 2004). In the second stage, PTE ions penetrate the cell membrane
104 and enter cells *via* active biosorption, and it is dependent on fungal metabolism and
105 related to the transportation and deposition of PTEs (Leonard et al., 2004).
106 Accordingly, from the eventual allocation of PTEs within cells, biosorption can be
107 classified as extracellular accumulation or precipitation, cell surface sorption or
108 precipitation, and intracellular accumulation (Veglio and Beolchini, 1997). However,
109 most previous studies address fungal PTE biosorption in rich or defined media with
110 limited carbon sources, not able to represent their phenotypic features and biosorption
111 performance in real-world scenarios, where the biosorption process is influenced by
112 many environmental variables, such as PTE availability, carbon sources and growth
113 conditions (Hamdy, 2000; He and Chen, 2014; Wang and Chen, 2014). It is of great
114 importance to inspect microbial phenotypic features and PTE biosorption capabilities
115 across a wide range of environmental conditions representing real-world scenarios,
116 and a reliable and high-throughput analytical method is urgently required.

117 Biospectroscopy as a group of interdisciplinary tools has many advantages in
118 microbiological study owing to their measurement attributes with a high-throughput,
119 nonintrusive and nondestructive manner (Heys et al., 2014; Jin et al., 2020; Jin et al.,
120 2017a; Li et al., 2017; Martin et al., 2010). Infrared (IR) spectroscopy, for instance,
121 relies on the principle that the energy from the infrared radiation is absorbed by the
122 bending, stretching and twisting of bonds (C-H, O-H, N-H, C=O, C-C, etc.) within the

123 sample, resulting in characteristic transmittance and reflectance patterns (Martin et al.,
124 2010; Naumann et al., 2005). Previous spectroscopic studies have successfully
125 detected the presence of fungal cells, characterized fungal species, and diagnosed
126 fungi-induced diseases (Gordon et al., 1999; Kos et al., 2002; Naumann et al., 2005).
127 Recently, biospectroscopic approaches are expanded to determine microbial
128 interactions with environmental stimuli, *e.g.*, antibiotic resistance (Jin et al., 2017a;
129 Jin et al., 2017b), showing great potentials in studying PTE-biosorption processes and
130 bringing new insights into the relevant mechanisms. Yet, no such attempt is reported.

131 The present study applied attenuated total reflection Fourier-transform infrared
132 (ATR-FTIR) spectroscopy coupled with phenotype microarrays to characterize the
133 biosorption of Cd and Pb by a fungal strain *Simplicillium chinense* QD10 cultivated
134 with 48 different carbon sources. This is the first study using spectrochemical tool to
135 analyse fungal PTE-biosorption process and investigate the impacts of carbon sources
136 in a high-throughput and nondestructive manner. Our results aimed to provide a
137 valuable spectroscopic database to look deeper into the biosorption mechanism from a
138 novel perspective and offer new clues to enhance fungi-associated phytoremediation
139 by altering the metabolic activities and biosorption performance of fungal cells in
140 real-world scenarios.

141 **2. Materials and Methods**

142 *2.1 Strains and cultivation condition*

143 The fungal strain *Simplicillium chinense* used in this study was isolated in soils from
144 Zhalong Wetland (47°32'30"N, 124°37'50"E, Qiqihar City, China) in October 2015. It
145 was named as *S. chinense* QD10 and had a satisfactory biosorption performance for
146 Cd and Pb (Jin et al., 2019). This strain was cultivated in potato dextrose medium

147 (200 g of potato, 20 g of glucose and 20 g of agarose dissolved in 1,000 mL of
148 deionized water and autoclaved) at 28°C for 5 days. Subsequently, the cells were
149 washed and resuspended in deionized water as stock solution for further treatment. Cd
150 and Pb stock solutions were prepared by dissolving $\text{Pb}(\text{NO}_3)_2$ and CdSO_4 in deionized
151 water, respectively. The final concentration of Cd and Pb in stock solution was 1.0
152 g/L.

153 PM1 plate (BIOLOG, Hayward, CA, USA) was used to examine the carbon metabolic
154 features of *S. chinense* QD10. Fifteen microliters of the cell stock solution were
155 resuspended in 135 μL of minimal medium (Zhang et al., 2011) and then added into
156 each well of a PM1 plate. Each well was then supplemented with 1.5 μL of Redox
157 Dye Mix A (100 \times , BIOLOG, Hayward, CA, USA) to monitor fungal growth. The
158 plate was incubated at 30°C for 5 days, and the colour development was measured
159 every 4 hours for the absorbance at 590 nm wavelength (respiratory unit, RU) by a
160 multimode microplate reader (FLUOstar Omega, BMG Labtech, UK). To avoid the
161 influence of Redox Dye on fungal biospectra, another treatment was prepared
162 following the same protocol except for the addition of Redox Dye Mix A, and used
163 for biospectral analysis. All the treatments were carried out in triplicates.

164 2.2 Cd/Pb biosorption treatment and chemical analysis

165 After 5-day cultivation, each well of PM1 plate was subjected with 20 μL of Pb or Cd
166 stock solution and kept shaking for 2 hours (final Pb or Cd concentration of 100
167 mg/L). Subsequently, the supernatant was collected after 3,000-rpm centrifugation for
168 20 min. The cell pellets were further washed with 5 mL deionized water and
169 centrifuged again (3,000 rpm) for another 20 min. The supernatants from two-step
170 centrifugation were combined, spiked with 20 μL of internal standards (^{103}Rh , ^{45}Sc ,

171 ^{209}Bi), and diluted with deionized water to a final volume of 50 mL for metal analysis.
172 Cd and Pb were analyzed by inductively coupled plasma mass spectrometry (ICP-MS,
173 X-series 2, Thermo Scientific, USA), and the detection wavelength was 228.8 and
174 283.3 nm, respectively. The standard calibration solution contained a mixture of Cd
175 and Pb in HNO_3 (0.1 M), ranging from 0 to 100 $\mu\text{g/L}$.

176 *2.3 Infrared spectra measurement*

177 Cell pellets after biosorption were further washed three times with sterile deionized
178 water to remove the residues of growth media and resuspended in 70% ethanol for
179 fixation. The washed cell pellets (minimal amount $>5 \mu\text{L}$) were applied onto Low-E
180 slides for interrogation by ATR-FTIR spectroscopy. A TENSOR 27 FTIR
181 spectrometer (Bruker Optics Ltd., UK) equipped with a Helios ATR attachment
182 (containing a diamond internal IRE; incidence angle of the IR beam: 45°) was used
183 and the instrument parameters were set as 32 scans and spatial resolution of 8 cm^{-1} .
184 Before the measurement of a new sample, the crystal was cleaned with deionized
185 water, and the background readings were retaken. A total of 20 spectra were acquired
186 for each treatment.

187 *2.4 Data analysis*

188 The RU of fungal cells was analysed by MARS software (BMG Labtech, UK). The
189 relative RU for fungal growth with each carbon source was calculated as the mean of
190 all RUs measured on day 5. The growth index (GI) of fungal cells cultivated with
191 different carbon source was calculated in Equation (1).

$$192 \quad \text{GI}_n = \frac{[\text{Relative RU}]_n}{[\text{Relative RU}]_{A1}} - 1.0 \quad (2)$$

193 Here, GI_n refers to the GI in n th well. $[\text{Relative RU}]_n$ and $[\text{Relative RU}]_{A1}$

194 represent the relative RU in n th well and well A1 (no carbon source, negative control),
195 respectively.

196 Fungal biomass was obtained by drying the cell pellets and measuring the weight with
197 the unit of dry cell weight (DCW). The linear regression between the GI and biomass
198 was obtained by serially diluted fungal suspension with the known GI and biomass,
199 following Equation (2).

$$200 \qquad \qquad \qquad \text{Biomass} = 0.196 \times \text{GI} + 0.168 \qquad (2)$$

201 The initial spectral data generated from ATR-FTIR spectroscopy were analyzed
202 within MATLAB R2011a software (TheMathsWorks, Natick, MA, USA), coupled
203 with IrootLab toolbox (<http://irootlab.googlecode.com>) (Trevisan et al., 2013). Unless
204 otherwise stated, the acquired spectra were truncated to the biochemical-cell
205 fingerprint region ($1800\text{-}900\text{ cm}^{-1}$), rubberband baseline corrected and normalized to
206 Amide I (1650 cm^{-1}) (Baker et al., 2014; Martin et al., 2010). Second order
207 differentiation baseline correction and vector normalization were also performed as an
208 alternative mean to process the data. Cross-calculation principal component analysis
209 followed by linear discriminant analysis (PCA-LDA) was subsequently applied to the
210 preprocessed data to reduce the number of spectra to 10 uncorrelated principal
211 components (PCs), which account for >99% of the total variance; LDA is a
212 supervised technique coupled with PCA in order to maximize inter-class and
213 minimize intra-class variance (Martin et al., 2010). To identify the specific IR bands
214 associated with fungal growth and biosorption efficiency of Pb or Cd, cluster vector
215 approach was conducted and visualized the discriminating difference (Butler et al.,
216 2015; Martin et al., 2010). The relationships between each IR band intensity and GI,
217 Pb biosorption efficiency or Cd biosorption efficiency across media supplemented

218 with 48 carbon sources were analysed by Pearson correlation analysis ($p < 0.05$). All
219 the statistical analyses were carried out in GraphPad Prism 6 unless specific
220 statement.

221 3. Results

222 3.1 *S. chinense* QD10 growth profiles cultivated with 48 carbon sources

223 The growth curves of *S. chinense* QD10 obtained from the RU measurement
224 illustrated significant differences across media supplemented with 48 carbon sources
225 (Figure 1A). In all treatments, an obvious lag phase lasted for about 8 hours, followed
226 by a dramatical increasing RU for some carbon sources. After the logarithmic growth
227 phase, *S. chinense* QD10 entered the stationary phase at 72 hours. These results
228 demonstrated that *S. chinense* QD10 could effectively utilize some carbon sources and
229 achieve satisfactory growth for 3 days. Figure 1B illustrated that the four carbon
230 sources possessing significantly higher GI (> 1.0) were L-glutamine, Tween 80,
231 glycolic acid and methylpyruvate. Fourteen carbon sources moderately supporting the
232 growth of *S. chinense* QD10 ($0.5 < GI < 1.0$) included α -hydroxyglutaric acid-g-lactone,
233 α -hydroxybutyric acid, adenosine, Gly-Asp, fumaric acid, bromosuccinic acid,
234 glyoxylic acid, D-cellobiose, inosine, Gly-Glu, tricarballic acid, p-hydroxyphenyl
235 acetic acid, m-hydroxyphenyl acetic acid, and 2-aminoethanol. Other carbon sources
236 were barely useable by *S. chinense* QD10 as the GI was < 0.5 . Based on the molecular
237 structure and functional groups, 48 carbon sources were categorized into five groups
238 as nucleic acids, carbohydrates, carboxylic acids, amino acids and others. There was
239 no significant difference in fungal growth between the five groups of carbon sources
240 ($p > 0.05$).

241 3.2 Cd and Pb biosorption by *S. chinense* QD10 cultivated with 48 different
242 carbon sources

243 Both Cd and Pb were efficiently adsorbed by *S. chinense* QD10 cultivated in minimal
244 medium with 48 different carbon sources, and the biosorption efficiency achieved >90%
245 for all treatments (Table S1 in Electronic Supporting Information, ESI). Two
246 adsorption equilibrium models (Langmuir and Freundlich) were applied to understand
247 Cd and Pb biosorption mechanisms by *S. chinense* QD10. The Langmuir isotherm
248 model represents the monolayer adsorption mechanism with a restriction of no
249 stacking of adsorbed molecules, as described in Equation (3). The Freundlich
250 isotherm model represents both monolayer and multilayer adsorptions by considering
251 the heterogeneous surfaces possessing different sorption energy sites, as described in
252 Equation (4).

$$253 \quad Q_e = Q_{max} \frac{K_L C_e}{1 + K_L C_e} \quad (3)$$

$$254 \quad Q_e = K_F C_e^{1/n} \quad (4)$$

255 Here, Q_e (mg/g DCW) refers to the total Cd/Pb biosorption capacity, and C_e (g/L)
256 represents the equilibrium Cd/Pb concentration in the liquid phase. Q_{max} (mg/g
257 DCW) is the maximum Cd/Pb biosorption capacity for monolayer adsorption in
258 Langmuir isotherm model, and K_L (L/mg) is the Langmuir constant associated with
259 adsorption energy. K_F (mg/g DCW) represents Cd/Pb biosorption capacity in both
260 monolayer and multilayer mechanism in Freundlich isotherm model, and $1/n$ is the
261 heterogeneous sorption sites. Either Langmuir or Freundlich isotherm model can be
262 expressed in a linear form as shown in Equations (5) and (6), respectively.

$$263 \quad \frac{C_e}{Q_e} = \frac{1}{Q_{max} K_L} + \frac{C_e}{Q_{max}} \quad (5)$$

$$\log Q_e = \log K_F + \frac{1}{n} \times \log C_e \quad (6)$$

265 Figure 2A illustrates that Cd biosorption fits better with Langmuir isotherm
266 ($R^2=0.7324$) than Freundlich isotherm ($R^2=0.0653$). The maximum Langmuir
267 biosorption capacity (Q_{max}) is 1.81 (mg/g DCW) and the Langmuir constant
268 associated with adsorption energy (K_L) is 1.75 L/mg. In contrast, Pb biosorption fits
269 better with Freundlich isotherm ($R^2=0.9458$) than Langmuir isotherm ($R^2=0.1121$,
270 Figure 2B). The empirical parameter related to heterogeneous sorption site ($1/n$) is
271 0.84 and the biosorption capacity (K_F) is 0.77 (mg/g DCW) in Freundlich isotherm.

272 *3.3 Infrared spectra of S. chinense QD10 cultivated with 48 different carbon* 273 *sources*

274 In general, *S. chinense* QD10 shared similar infrared spectra across 48 different
275 carbon sources regarding the cellular structures (Figure 3A), including lipid (~ 1750
276 cm^{-1}), Amide I (~ 1650 cm^{-1}), Amide II (~ 1550 cm^{-1}), Amide III (~ 1260 cm^{-1}),
277 carbohydrate (~ 1155 cm^{-1}) and symmetric phosphate stretching vibrations (~ 1080
278 cm^{-1}). The 1D score plot of PCA-LDA (Figure 3B) indicated the variations between
279 each category of carbon source, and one-way ANOVA test coupled with Turkey's
280 multiple comparisons demonstrated that the biospectra in the five groups of carbon
281 sources were significantly differentiated ($p<0.05$), except for the variation between
282 the groups of amino acids and others ($p>0.05$).

283 The cluster vector analysis reveals more information regarding the biomolecular
284 difference (Figure 4), which includes five primary peaks derived from original spectra
285 as relevant biomarkers for each group of carbon sources. More precisely, the
286 biomarkers of *S. chinense* QD10 cultivated with amino acids are (~1134 cm^{-1}), PO_2^-
287 asymmetric (~ 1265 cm^{-1}), Amide III (~ 1185 cm^{-1}), Amide II (~ 1517 cm^{-1}) and C=O

288 (~ 1728 cm^{-1}). Besides the peak of PO_2^- asymmetric (~ 1265 cm^{-1}), other significant
289 peaks of carbohydrate-cultivated *S. chinense* QD10 cells are RNA (~ 1117 cm^{-1}), CH
290 in-plane bend (~ 1510 cm^{-1}), Amide I (~ 1659 cm^{-1}) and C=O, lipids (~ 1740 cm^{-1}). In
291 nucleic acid group, the characteristic peaks are $\nu(\text{CO})$, $\nu(\text{CC})$ (~ 1018 cm^{-1}),
292 deoxyribose (~ 1188 cm^{-1}), (~ 1269 cm^{-1}), Amide II (~ 1540 cm^{-1}) and lipids (~ 1740
293 cm^{-1}). For carboxylic acid group, the characteristic peaks include stretching vibrations
294 of hydrogen-bonding, C-OH groups (~ 1153 cm^{-1}), N-H thymine (~ 1276 cm^{-1}), C=C,
295 deformation C-H (~ 1496 cm^{-1}), Ring base (~ 1555 cm^{-1}), base carbonyl stretching
296 and ring breathing mode (~ 1620 cm^{-1}). Characteristic peaks for other carbon sources
297 include stretching C-O deoxyribose (~ 1056 cm^{-1}), C-O stretching vibration (~ 1150
298 cm^{-1}), PO_2^- asymmetric (~ 1256 cm^{-1}), ring base (~ 1555 cm^{-1}) and lipids (~ 1740
299 cm^{-1}).

300 *3.4 Mechanisms of Cd and Pb biosorption via spectral analysis*

301 As fungal PTE-biosorption consists of two key stages as direct adsorption on fungal
302 membrane and penetration through cell wall, they might be distinguished by
303 analyzing the functional groups of cellular components or extracellular polymeric
304 substance (EPS). Although PCA-LDA is applied to assess the ‘fingerprint region’ to
305 characterize the relationships between the whole biospectra and fungal growth or
306 biosorption efficiency, it is very challenging because the enormous spectral alterations
307 across 48 different carbon sources (Figure 5A). We therefore attempted to identify
308 discriminating alterations by introducing Pearson correlations to determine the
309 relationships between microbial activities (e.g., biomass, Pb biosorption, Cd
310 biosorption) and spectral variations based on cluster vector analysis. The results
311 indicated that several discriminating alterations positively correlated with fungal
312 biomass (Figure 5A), including 1340 cm^{-1} (collagen, $p < 0.05$), 1136 cm^{-1} (collagen,

313 $p < 0.05$) and 966 cm^{-1} (C-C DNA, $p < 0.05$). These peaks could be viewed as
314 biomarkers for fungal growth (Figure 5B-5D). The significant peaks associated with
315 Cd biosorption included 1745 cm^{-1} (phospholipids, $p < 0.05$), 1620 cm^{-1} (nucleic acid,
316 $p < 0.05$), 1456 cm^{-1} (lipids and proteins, $p < 0.05$), 1396 cm^{-1} (proteins, $p < 0.05$) and
317 1057 cm^{-1} (stretching C-O deoxyribose, $p < 0.05$), as illustrated in Figure 5E-5I.
318 However, there was no biomarker correlated with Pb biosorption, further confirming
319 the different biosorption mechanisms between Cd and Pb as suggested by the results
320 of biosorption isotherms.

321 4. Discussion

322 4.1 Biosorption capability of *S. chinense* QD10 on Cd and Pb

323 Previous studies investigating microbes as biosorbents have demonstrated strong
324 capacities of microbial cells to absorb and remove PTEs, such as marine algae and
325 yeasts (Goyal et al., 2003; Özer and Özer, 2003; Volesky and Holan, 1995; Wang and
326 Chen, 2006). *Ascophyllum* and *Sargassum*, which can accumulate PTEs more than 30%
327 of dry weight biomass (Volesky and Holan, 1995). *Saccharomyces Cerevisiae* is a
328 species belonging to yeast, whose PTE biosorption capability ranges from 10 to 300
329 mg/g DCW for Pb and 10 to 100 mg/g DCW for Cd from the equilibrium biosorption
330 processes (Wang and Chen, 2006). PTE biosorption by fungi has also been
331 investigated, such as *Penicillium* sp. MRF-1 which has a strong biosorption capacity
332 of Cd (0.13-9.39 mg/g DCW) (Velmurugan et al., 2010) and *Exiguobacterium* sp.
333 with a maximum biosorption capacity of 15.6 mg/g DCW for Cd in Langmuir
334 isotherm (Park and Chon, 2016). In the present study, the biosorption capacity of *S.*
335 *chinense* QD10 was 0.77 mg/g DCW for Pb and 1.81 mg/g DCW for Cd, much lower
336 than a previous report on the same strain in rich medium (24.6 mg/g DCW for Cd and

337 31.2 mg/g DCW for Pb) (Jin et al., 2019). It might be attributing to the defined
338 medium used in this study, which is nutrient deficient and cannot support the best
339 fungal growth. Accordingly, fungal cells might not achieve optimal activities,
340 resultings in limited active binding sites on fungal cell membrane and lower Cd/Pb
341 biosorption capacity by *S. chinense* QD10. However, defined medium fits better with
342 the real scenarios in natural habitats, where microbes survive under nutrient depletion
343 conditions (Jin et al., 2017a; Jin et al., 2018a). Our result provides a high-throughput
344 and more comprehensive database to evaluate the PTE-biosorption performance of *S.*
345 *chinense* QD10 regarding phytoremediation practices.

346 4.2 Biospectral fingerprints of *S. chinense* QD10

347 Biospectroscopy has a long history of studying biological cells. IR spectroscopy can
348 be traced back to 1950s (Jin et al., 2017b) and has been extensively applied as a
349 sensitive and rapid screening tool for characterizing microbes (Jin et al., 2017b;
350 Picorel et al., 1991). Over the past 20 years, IR spectroscopy is successfully
351 developed for examining biological molecules at cell or tissue level, including
352 bacteria, yeast and mammalian cells (Baker et al., 2014; Martin et al., 2010;
353 Movasaghi et al., 2008). However, only limited works focus on fungi, and there is
354 lack of well-established database for fungal spectral biomarkers. In the present study,
355 our results illustrated similar biospectra with several key biomarkers of fungi
356 comparing to those of bacterial cells based on past literatures, including lipid (~ 1750
357 cm^{-1}), Amide I (~ 1650 cm^{-1}), Amide II (~ 1550 cm^{-1}), carbohydrate (~ 1155 cm^{-1}) and
358 symmetric phosphate stretching vibrations (~ 1080 cm^{-1}) (Baker et al., 2014;
359 Maquelin et al., 2003; Martin et al., 2010). It might be attributed to the similar cell
360 wall components, such as lipids, proteins and carbohydrate, even though fungi are
361 protected by a true cell wall (Sağ, 2001).

362 4.3 Spectral biomarkers for *S. chinense* QD10 growth across carbon source
363 groups

364 Although the GI of *S. chinense* QD10 cultivated with different carbon source groups
365 showed no significant difference, the cluster vector analysis raises more biochemical
366 information by locating the discriminating biomarkers across carbon source categories.
367 These biomarkers reveal the metabolic features of *S. chinense* QD10 responsive to
368 carbon sources. Cultivated with carbohydrate, for instance, biospectra of *S. chinense*
369 QD10 have specific biomarkers including PO₂⁻ asymmetric (~ 1265 cm⁻¹), RNA (~
370 1117 cm⁻¹), CH in-plane bend (~ 1510 cm⁻¹), Amide I (~ 1659 cm⁻¹) and C=O, lipids
371 (~ 1740 cm⁻¹), indicating the occurrence of complex carbohydrate metabolic
372 processes during fungal growth (Figure 4). These biomarkers are significantly
373 different from those linked with bacterial growth except for Amide I (~ 1659 cm⁻¹)
374 (Jin et al., 2018a; Jin et al., 2018b), suggesting distinct metabolite profiles between
375 fungal and bacterial growth. Carbohydrates are reported to associate with fungal
376 metabolism, not only providing energy for the synthesis of trehalose, polyols,
377 glycogen, fatty acids and other cellular components, but also supplying carbon
378 skeleton for other metabolic processes, such as hyphal growth and amino acid
379 biosynthesis (Bago et al., 2003; Deveau et al., 2008; Rasmussen et al., 2008). As the
380 fungal metabolisms vary across intra- and inter-groups of different carbon sources
381 throughout the growth period, there is no clear relationship between growth and
382 carbon source categories.

383 We further applied Pearson correlation analysis based on cluster vector analysis to
384 link the spectral variations with fungal biomass and identify some key biomarkers for
385 fungal growth. The IR bands significantly correlated with GI include 1340 cm⁻¹
386 (collagen), 1136 cm⁻¹ (collagen) and 966 cm⁻¹ (C-C DNA, Figure 5B-5D), implying

387 strong associations of these cellular components with fungal growth. Among them,
388 the DNA-spectral biomarker represents DNA replication through cell reproduction
389 process (Jin et al., 2018a; Jin et al., 2018b). Additionally, the collagen-associated
390 spectral alterations are very likely linked to the formation of fungal fimbriae, which
391 consist of collagen and are abundant on extracochlear surfaces (Celerin et al., 1996).
392 Our results suggest that these spectral biomarkers can be used as fungal growth
393 indicators in future studies.

394 *4.4 Derived biospectral biomarkers explaining different mechanisms of Cd and* 395 *Pb biosorption*

396 Cultivated with different carbon sources, Cd and Pb biosorption by *S. chinense* QD10
397 followed the Langmuir and Freundlich isotherm, respectively. It implied distinct
398 mechanisms behind Pb and Cd biosorption, consistent with our previous report (Jin et
399 al., 2019). As the Langmuir isotherm represents the monolayer adsorption mechanism
400 and the Freundlich isotherm describes both monolayer and multilayer adsorptions by
401 considering the heterogeneous surfaces possessing different sorption energy sites,
402 spectrochemical analysis might provide deeper insights *via* diagnosing spectral
403 alterations associated with PTE biosorption process.

404 The results of spectral analysis indicate that phosphor-lipids and proteins (1745 cm^{-1} ,
405 1456 cm^{-1} , 1396 cm^{-1}) are strongly correlated with Cd biosorption (Figure 5E-5I). It
406 suggests that the cell wall components of *S. chinense* QD10 are the primary
407 interactive targets for Cd biosorption, such as polysaccharides, proteins and lipids
408 which offer abundant metal-binding functional groups, *e.g.*, carboxylate hydroxyl,
409 sulphate, phosphate and amino groups (Veglio and Beolchini, 1997). It is consistent
410 with the fact that Cd biosorption isotherm follows the Langmuir isotherm and is more

411 likely driven by the cell surface sorption that both proteins and carbohydrate fractions
412 are involved in the binding of Cd ions (Jin et al., 2019). In contrast, no spectral
413 biomarker is observed to significantly associate with Pb biosorption. This result is
414 also evidenced by the Freundlich isotherm of Pb biosorption describing both
415 monolayer and multilayer adsorptions by considering the heterogeneous surfaces.
416 Thus, it suggests that extracellular precipitation explains the majority of Pb
417 biosorption and EPS possess a substantial quantity of anion functional groups
418 adsorbing Pb^{2+} ions (Wang and Chen, 2006).

419 This discrimination may be derived from the two stages of PTE biosorption
420 mechanisms by fungi: direct adsorption on fungal membrane and penetration through
421 cell wall (Leonard et al., 2004). These two stages can occur independently, possibly
422 resulting in distinct biosorption behaviour across biosorbents (microbial species) or
423 PTEs. For instance, exopolysaccharides (EPS) represent an interesting affinity for Pb,
424 which is a metabolism-independent process driven by interactions between the cations
425 and negative charges of acidic functional groups of EPS (Pérez et al., 2008). As EPS
426 are a mixture of biomaterials, such as EPS, glucoprotein, lipopolysaccharide and
427 soluble peptide (Jin et al., 2019), it is very challenging to distinguish and extract
428 specific spectral biomarkers associated with extracellular components responsible for
429 PTE biosorption. Our results hint that discriminating peaks derived from IR spectra
430 could satisfactorily uncover the behaviour and mechanisms of PTE biosorption by
431 interrogating the distinct functional groups or cellular components (Martin et al.,
432 2010).

433 **5. Conclusion and remarks**

434 Fungi-assisted phytoremediation is an environmentally-safe approach to remove PTEs

435 from contaminated soils, and PTE biosorption by fungi is a critical step in
436 phytoremediation. This study introduced ATR-FTIR spectroscopy coupled with
437 Biolog PM plate as a non-destructive and high-throughput approach to investigate the
438 performance and mechanisms of Cd and Pb biosorption by a fungal strain *S. chinense*
439 QD10 cultivated with difference carbon sources. For the first time, we found several
440 spectral biomarkers associated with the growth (1340 cm^{-1} , 1136 cm^{-1} , 966 cm^{-1}) and
441 Cd biosorption (1745 cm^{-1} , 1620 cm^{-1} , 1456 cm^{-1} , 1396 cm^{-1} , 1057 cm^{-1}) of *S.*
442 *chinense* QD10. Cd biosorption primarily followed the monolayer Langmuir isotherm
443 and was mainly driven by the cell surface sorption, unravelled by the spectral
444 alterations affiliated with proteins and carbohydrates (1745 cm^{-1} , 1456 cm^{-1} , 1396
445 cm^{-1}). For Pb biosorption, EPS possibly possessed a substantial quantity of anion
446 functional groups adsorbing Pb^{2+} ions as extracellular precipitation, thus following
447 multilayer Freundlich isotherm and representing no significant spectral biomarkers.
448 Our results suggested biospectroscopy as a powerful tool in investigating the
449 interactions between fungal cells and PTEs, distinguishing both functional groups and
450 mechanisms associated with PTE biosorption process. This study lends new sights
451 into fungal PTE biosorption and offers database of their behaviour across various
452 carbon sources, revealing the tip of the iceberg regarding the interactions between
453 microbes and PTEs in real-world scenario from spectroscopic perspective, which
454 implies great potential for enhancing phytoremediation.

455 **6. Declaration of Competing Interest**

456 The authors declare that they have no known competing financial interests or personal
457 relationships that could have appeared to influence the work reported in this paper.

458 7. Acknowledgements

459 This study was supported by the National Key Research and Development Program of
460 China (2018YFC1800701), Natural Science Foundation of China (No. 41977346),
461 China Postdoctoral Science Foundation (2019M650707), Natural Science Foundation
462 of Heilongjiang Province (No. C201240) and Science and Technology Research
463 Project of the Department of Education, Heilongjiang Province (No. 12531754). DZ
464 also acknowledges the support of Chinese Government's Thousand Talents Plan for
465 Young Professionals.

466

467 **8. Reference**

- 468 Ali, H., Khan, E., Sajad, M.A., 2013. Phytoremediation of heavy metals-Concepts and
469 applications. *Chemosphere* 91, 869-881.
- 470 Bago, B., Pfeffer, P.E., Abubaker, J., Jun, J., Allen, J.W., Brouillette, J., Doudu, D.D.,
471 Lammers, P.J., Shachar-Hill, Y., 2003. Carbon export from arbuscular mycorrhizal
472 roots involves the translocation of carbohydrate as well as lipid. *Plant Physiol* 131,
473 1496-1507.
- 474 Baker, M.J., Trevisan, J., Bassan, P., Bhargava, R., Butler, H.J., Dorling, K.M.,
475 Fielden, P.R., Fogarty, S.W., Fullwood, N.J., Heys, K.A., Hughes, C., Lasch, P.,
476 Martin-Hirsch, P.L., Obinaju, B., Sockalingum, G.D., Sule-Suso, J., Strong, R.J.,
477 Walsh, M.J., Wood, B.R., Gardner, P., Martin, F.L., 2014. Using Fourier transform IR
478 spectroscopy to analyze biological materials. *Nat Protoc* 9, 1771-1791.
- 479 Bolan, N., Kunhikrishnan, A., Thangarajan, R., Kumpiene, J., Park, J., Makino, T.,
480 Kirkham, M.B., Scheckel, K., 2014. Remediation of heavy metal(loid)s contaminated
481 soils - To mobilize or to immobilize? *J Hazard Mater* 266, 141-166.
- 482 Butler, H.J., McAinsh, M.R., Adams, S., Martin, F.L., 2015. Application of vibrational
483 spectroscopy techniques to non-destructively monitor plant health and development.
484 *Anal Methods* 7, 4059-4070.
- 485 Celerin, M., Ray, J.M., Schisler, N.J., Day, A.W., Stetler-Stevenson, W.G.,
486 Laudenschlager, D., 1996. Fungal fimbriae are composed of collagen. *Embo J.* 15, 4445.
- 487 Deng, S., Ke, T., Li, L., Cai, S., Zhou, Y., Liu, Y., Guo, L., Chen, L., Zhang, D., 2018a.
488 Impacts of environmental factors on the whole microbial communities in the
489 rhizosphere of a metal-tolerant plant: *Elsholtzia haichowensis* Sun. *Environ. Pollut.*
490 237, 1088-1097.
- 491 Deng, S.Q., Ke, T., Wu, Y.F., Zhang, C., Hu, Z.Q., Yin, H.M., Guo, L.M., Chen, L.Z.,
492 Zhang, D.Y., 2018b. Heavy Metal Exposure Alters the Uptake Behavior of 16 Priority
493 Polycyclic Aromatic Hydrocarbons (PAHs) by Pak Choi (*Brassica chinensis* L.).
494 *Environ Sci Technol* 52, 13457-13468.
- 495 Deveau, A., Kohler, A., Frey-Klett, P., Martin, F., 2008. The major pathways of
496 carbohydrate metabolism in the ectomycorrhizal basidiomycete *Laccaria bicolor*
497 S238N. *New Phytol* 180, 379-390.
- 498 Dong, X.Q., Li, C.L., Li, J., Wang, J.X., Liu, S.T., Ye, B., 2010. A novel approach for
499 soil contamination assessment from heavy metal pollution: A linkage between
500 discharge and adsorption. *J Hazard Mater* 175, 1022-1030.
- 501 Geelhoed, J.S., Meeussen, J.C.L., Roe, M.J., Hillier, S., Thomas, R.P., Farmer, J.G.,
502 Paterson, E., 2003. Chromium remediation or release? Effect of iron(II) sulfate
503 addition on chromium(VI) leaching from columns of chromite ore processing residue.
504 *Environ Sci Technol* 37, 3206-3213.
- 505 Gheju, M., Balcu, I., Mosoarca, G., 2016. Removal of Cr(VI) from aqueous solutions
506 by adsorption on MnO₂. *J Hazard Mater* 310, 270-277.
- 507 Gordon, S., Jones, R., McClelland, J., Wicklow, D., Greene, R., 1999. Transient
508 infrared spectroscopy for detection of toxigenic fungi in corn: potential for on-line
509 evaluation. *J Agr Food Chem* 47, 5267-5272.

- 510 Goyal, N., Jain, S., Banerjee, U., 2003. Comparative studies on the microbial
511 adsorption of heavy metals. *Adv Environ Res* 7, 311-319.
- 512 Hamdy, A., 2000. Biosorption of heavy metals by marine algae. *Curr Microbiol* 41,
513 232-238.
- 514 He, J., Chen, J.P., 2014. A comprehensive review on biosorption of heavy metals by
515 algal biomass: materials, performances, chemistry, and modeling simulation tools.
516 *Bioresour Technol* 160, 67-78.
- 517 Heys, K.A., Riding, M.J., Strong, R.J., Shore, R.F., Pereira, M.G., Jones, K.C.,
518 Semple, K.T., Martin, F.L., 2014. Mid-infrared spectroscopic assessment of
519 nanotoxicity in gram-negative vs. gram-positive bacteria. *Analyst* 139, 896-905.
- 520 Huang, Y., Wang, L., Wang, W., Li, T., He, Z., Yang, X., 2019. Current status of
521 agricultural soil pollution by heavy metals in China: A meta-analysis. *Sci Total*
522 *Environ* 651, 3034-3042.
- 523 Järup, L., 2003. Hazards of heavy metal contamination. *Brit Med Bull* 68, 167-182.
- 524 Jiang, B., Adebayo, A., Jia, J., Xing, Y., Deng, S.Q., Guo, L.M., Liang, Y.T., Zhang,
525 D.Y., 2019. Impacts of heavy metals and soil properties at a Nigerian e-waste site on
526 soil microbial community. *J Hazard Mater* 362, 187-195.
- 527 Jiang, B., Xing, Y., Zhang, B.G., Cai, R.Q., Zhang, D.Y., Sun, G.D., 2018. Effective
528 phytoremediation of low-level heavy metals by native macrophytes in a vanadium
529 mining area, China. *Environ Sci Pollut R* 25, 31272-31282.
- 530 Jin, N., Morais, C.L.M., Martin, F.L., Zhang, D., 2020. Spectrochemical identification
531 of kanamycin resistance genes in artificial microbial communities using Clover-assay.
532 *J Pharmaceut Biomed* 181, 113108.
- 533 Jin, N., Paraskevaidi, M., Semple, K.T., Martin, F.L., Zhang, D.Y., 2017a. Infrared
534 Spectroscopy Coupled with a Dispersion Model for Quantifying the Real-Time
535 Dynamics of Kanamycin Resistance in Artificial Microbiota. *Anal Chem* 89,
536 9814-9821.
- 537 Jin, N.F., Semple, K.T., Jiang, L.F., Luo, C.L., Martin, F.L., Zhang, D.Y., 2018a.
538 Spectrochemical determination of unique bacterial responses following long-term
539 low-level exposure to antimicrobials. *Anal Methods* 10, 1602-1611.
- 540 Jin, N.F., Semple, K.T., Jiang, L.F., Luo, C.L., Zhang, D.Y., Martin, F.L., 2018b.
541 Spectrochemical analyses of growth phase-related bacterial responses to low
542 (environmentally-relevant) concentrations of tetracycline and nanoparticulate silver.
543 *Analyst* 143, 768-776.
- 544 Jin, N.F., Zhang, D.Y., Martin, F.L., 2017b. Fingerprinting microbiomes towards
545 screening for microbial antibiotic resistance. *Integrative Biology* 9, 406-417.
- 546 Jin, Z., Deng, S., Wen, Y., Jin, Y., Pan, L., Zhang, Y., Black, T., Jones, K.C., Zhang, H.,
547 Zhang, D., 2019. Application of *Simplicillium chinense* for Cd and Pb biosorption and
548 enhancing heavy metal phytoremediation of soils. *Sci Total Environ* 697, 134148.
- 549 Khan, A.A., Muthukrishnan, M., Guha, B.K., 2010. Sorption and transport modeling
550 of hexavalent chromium on soil media. *J Hazard Mater* 174, 444-454.
- 551 Khan, A.G., 2005. Role of soil microbes in the rhizospheres of plants growing on
552 trace metal contaminated soils in phytoremediation. *J Trace Elem Med Bio* 18,
553 355-364.

- 554 Kos, G., Lohninger, H., Krska, R., 2002. Fourier transform mid-infrared spectroscopy
555 with attenuated total reflection (FT-IR/ATR) as a tool for the detection of *Fusarium*
556 fungi on maize. *Vib Spectrosc* 29, 115-119.
- 557 Leonard, S.S., Harris, G.K., Shi, X.L., 2004. Metal-induced oxidative stress and
558 signal transduction. *Free Radical Bio Med* 37, 1921-1942.
- 559 Li, H.B., Martin, F.L., Zhang, D.Y., 2017. Quantification of Chemotaxis-Related
560 Alkane Accumulation in *Acinetobacter baylyi* Using Raman Microspectroscopy. *Anal.*
561 *Chem.* 89, 3909-3918.
- 562 Liu, M., Qiao, G., Jiang, J., Han, X., Sang, J., Zhuo, R., 2014. Identification and
563 expression analysis of salt-responsive genes using a comparative microarray approach
564 in *Salix matsudana*. *Mol Biol Rep* 41, 6555-6568.
- 565 Liu, M.Y., He, X.L., Feng, T.Y., Zhuo, R.Y., Qiu, W.M., Han, X.J., Qao, G.R., Zhang,
566 D.Y., 2019. cDNA Library for Mining Functional Genes in *Sedum alfredii* Hance
567 Related to Cadmium Tolerance and Characterization of the Roles of a Novel SaCTP2
568 Gene in Enhancing Cadmium Hyperaccumulation. *Environ Sci Technol* 53,
569 10926-10940.
- 570 Liu, X.M., Song, Q.J., Tang, Y., Li, W.L., Xu, J.M., Wu, J.J., Wang, F., Brookes, P.C.,
571 2013. Human health risk assessment of heavy metals in soil-vegetable system: A
572 multi-medium analysis. *Sci Total Environ* 463, 530-540.
- 573 Maquelin, K., Kirschner, C., Choo-Smith, L.-P., Ngo-Thi, N., Van Vreeswijk, T.,
574 Stämmeler, M., Endtz, H., Bruining, H., Naumann, D., Puppels, G., 2003. Prospective
575 study of the performance of vibrational spectroscopies for rapid identification of
576 bacterial and fungal pathogens recovered from blood cultures. *J Clin Microbiol* 41,
577 324-329.
- 578 Martin, F.L., Kelly, J.G., Llabjani, V., Martin-Hirsch, P.L., Patel, I.I., Trevisan, J.,
579 Fullwood, N.J., Walsh, M.J., 2010. Distinguishing cell types or populations based on
580 the computational analysis of their infrared spectra. *Nat. Protoc.* 5, 1748-1760.
- 581 Movasaghi, Z., Rehman, S., ur Rehman, D.I., 2008. Fourier Transform Infrared (FTIR)
582 Spectroscopy of Biological Tissues. *Appl Spectrosc Rev* 43, 134-179.
- 583 Naumann, A., Navarro-González, M., Peddireddi, S., Kües, U., Polle, A., 2005.
584 Fourier transform infrared microscopy and imaging: Detection of fungi in wood.
585 *Fungal Genet Biol* 42, 829-835.
- 586 Ou, J., Li, H., Yan, Z., Zhou, Y., Bai, L., Zhang, C., Wang, X., Chen, G., 2018. In situ
587 immobilisation of toxic metals in soil using Maifan stone and illite/smectite clay. *Sci*
588 *Rep* 8, 1-9.
- 589 Özer, A., Özer, D., 2003. Comparative study of the biosorption of Pb (II), Ni (II) and
590 Cr (VI) ions onto *S. cerevisiae*: determination of biosorption heats. *J Hazard Mater*
591 100, 219-229.
- 592 Pérez, J.A.M., García-Ribera, R., Quesada, T., Aguilera, M., Ramos-Cormenzana, A.,
593 Monteoliva-Sánchez, M., 2008. Biosorption of heavy metals by the
594 exopolysaccharide produced by *Paenibacillus jamilae*. *World J Microbiol Biotechnol*
595 24, 2699.
- 596 Park, J.H., Chon, H.-T., 2016. Characterization of cadmium biosorption by
597 *Exiguobacterium* sp. isolated from farmland soil near Cu-Pb-Zn mine. *Environ Sci*

- 598 Pollut R 23, 11814-11822.
- 599 Patterson, R.R., Fendorf, S., Fendorf, M., 1997. Reduction of hexavalent chromium
600 by amorphous iron sulfide. *Environ Sci Technol* 31, 2039-2044.
- 601 Picorel, R., Holt, R.E., Heald, R., Cotton, T.M., Seibert, M., 1991. Stability of Isolated
602 Bacterial and Photosystem-II Reaction Center Complexes on Ag Electrode Surfaces -
603 a Surface-Enhanced Resonance Raman-Study. *J Am Chem Soc* 113, 2839-2843.
- 604 Rasmussen, S., Parsons, A.J., Fraser, K., Xue, H., Newman, J.A., 2008. Metabolic
605 profiles of *Lolium perenne* are differentially affected by nitrogen supply, carbohydrate
606 content, and fungal endophyte infection. *Plant Physiol* 146, 1440-1453.
- 607 Rui, D., Wu, Z., Ji, M., Liu, J., Wang, S., Ito, Y., 2019. Remediation of Cd- and Pb-
608 contaminated clay soils through combined freeze-thaw and soil washing. *J Hazard*
609 *Mater* 369, 87-95.
- 610 Sağ, Y., 2001. Biosorption of heavy metals by fungal biomass and modeling of fungal
611 biosorption: a review. *Sep Purif Methods* 30, 1-48.
- 612 Sarkar, B., Xi, Y., Megharaj, M., Krishnamurti, G.S.R., Rajarathnam, D., Naidu, R.,
613 2010. Remediation of hexavalent chromium through adsorption by bentonite based
614 Arquad®2HT-75 organoclays. *J Hazard Mater* 183, 87-97.
- 615 Say, R., Denizli, A., Arıca, M.Y., 2001. Biosorption of cadmium (II), lead (II) and
616 copper (II) with the filamentous fungus *Phanerochaete chrysosporium*. *Bioresour*
617 *Technol* 76, 67-70.
- 618 Sha, H., Wu, Y., Fan, Y., 2018. Utilization of industrial waste as a novel adsorbent:
619 Mono/competitive adsorption of chromium(VI) and nickel(II) using diatomite waste
620 modified by EDTA. *Appl Organomet Chem* 32, e3977.
- 621 Shaheen, S.M., Wang, J.X., Swertz, A.C., Feng, X.B., Bolan, N., Rinklebe, J., 2019.
622 Enhancing phytoextraction of potentially toxic elements in a polluted floodplain soil
623 using sulfur-impregnated organoclay. *Environ Pollut* 248, 1059-1066.
- 624 Singh, R., Dong, H., Zeng, Q., Zhang, L., Rengasamy, K., 2017. Hexavalent
625 chromium removal by chitosan modified-bioreduced nontronite. *Geochim*
626 *Cosmochim Acta* 210, 25-41.
- 627 Tantawy, M.A., El-Roudi, A.M., Salem, A.A., 2012. Immobilization of Cr(VI) in
628 bagasse ash blended cement pastes. *Construction and Building Materials* 30, 218-223.
- 629 Trevisan, J., Angelov, P.P., Scott, A.D., Carmichael, P.L., Martin, F.L., 2013. IRootLab:
630 a free and open-source MATLAB toolbox for vibrational biospectroscopy data
631 analysis. *Bioinformatics* 29, 1095-1097.
- 632 Veglio, F., Beolchini, F., 1997. Removal of metals by biosorption: a review.
633 *Hydrometallurgy* 44, 301-316.
- 634 Velmurugan, N., Hwang, G., Sathishkumar, M., Choi, T.K., Lee, K.-J., Oh, B.-T., Lee,
635 Y.-S., 2010. Isolation, identification, Pb (II) biosorption isotherms and kinetics of a
636 lead adsorbing *Penicillium* sp. MRF-1 from South Korean mine soil. *J Environ*
637 *Sci-China* 22, 1049-1056.
- 638 Volesky, B., Holan, Z., 1995. Biosorption of heavy metals. *Biotechnol Progr* 11,
639 235-250.
- 640 Wang, J., Chen, C., 2006. Biosorption of heavy metals by *Saccharomyces cerevisiae*:
641 a review. *Biotechnol Adv* 24, 427-451.

- 642 Wang, J., Chen, C., 2014. Chitosan-based biosorbents: modification and application
643 for biosorption of heavy metals and radionuclides. *Bioresour Technol* 160, 129-141.
- 644 Wang, S., Vipulanandan, C., 2001. Solidification/stabilization of Fe(II)-treated
645 Cr(VI)-contaminated soil. *Environ Eng Sci* 18, 301-308.
- 646 Wiszniewska, A., Hanus-Fajerska, E., Muszynska, E., Ciarkowska, K., 2016. Natural
647 Organic Amendments for Improved Phytoremediation of Polluted Soils: A Review of
648 Recent Progress. *Pedosphere* 26, 1-12.
- 649 Yan, G., Viraraghavan, T., 2003. Heavy-metal removal from aqueous solution by
650 fungus *Mucor rouxii*. *Water Res* 37, 4486-4496.
- 651 Yin, H., Niu, J., Ren, Y., Cong, J., Zhang, X., Fan, F., Xiao, Y., Zhang, X., Deng, J.,
652 Xie, M., He, Z., Zhou, J., Liang, Y., Liu, X., 2015. An integrated insight into the
653 response of sedimentary microbial communities to heavy metal contamination. *Sci*
654 *Rep* 5, 14266.
- 655 Yuan, W.Y., Xu, W.T., Wu, Z.B., Zhang, Z.W., Wang, L.C., Bai, J.F., Wang, X.Y.,
656 Zhang, Q.W., Zhu, X.F., Zhang, C.L., Wang, J.W., 2018. Mechanochemical treatment
657 of Cr(VI) contaminated soil using a sodium sulfide coupled solidification/stabilization
658 process. *Chemosphere* 212, 540-547.
- 659 Zhang, D., Fakhrullin, R.F., Özmen, M., Hui, W., Jian, W., Paunov, V.N., Li, G.,
660 Huang, W.E., 2011. Functionalization of whole cell bacterial reporters with magnetic
661 nanoparticles. *Microb Biotechnol* 4, 89-97.
- 662
- 663

664 9. Figure Captions

665 **Figure 1.** Growth profiles of *S. chinense* QD10 with 48 different carbon sources. (A)
666 Growth curves during a 144-hour cultivation period. (B) Growth indices (GI) of *S.*
667 *chinense* QD10 in comparison with the negative control (A1, no carbon source).

668 **Figure 2.** Cd and Pb adsorption isotherms by *S. chinense* QD10 cultivated with 48
669 different carbon sources. (A) Langmuir isotherm model representing the monolayer
670 adsorption mechanism. (B) Freundlich isotherm model representing both monolayer
671 and multilayer adsorptions by considering the heterogeneous surfaces possessing
672 different sorption energy sites. Initial concentration of Cd and Pb was 100 mg/L and
673 the adsorption time was 2 hours.

674 **Figure 3.** (A) Mean spectra of all pre-processed data of *S. chinense* QD10 cultivated
675 with 48 different carbon sources based on rubberband baseline correction and Amide I
676 (1650 cm^{-1}) normalization. (B) PCA-LDA categorizations of *S. chinense* QD10
677 cultivated with five groups of carbon sources, including nucleic acid, carbohydrate,
678 carboxylic acid, amino acid and others. Twenty infrared spectra were randomly
679 obtained per treatment. Different small letters indicate significant difference
680 (Duncan's test, $p < 0.05$) among treatments.

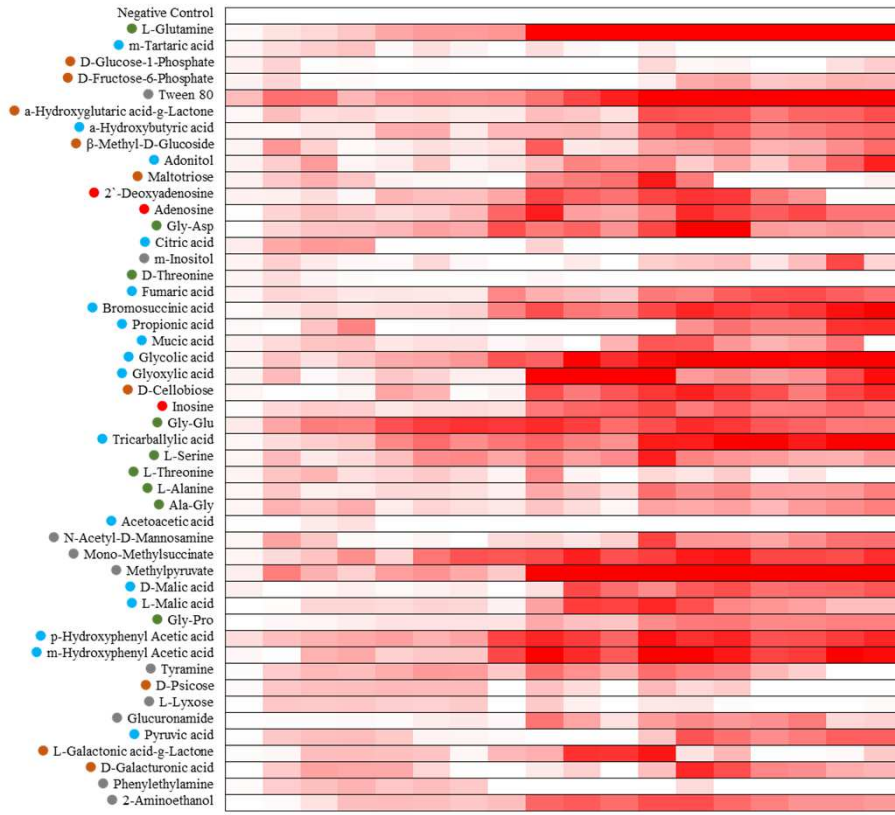
681 **Figure 4.** Cluster vector analysis of *S. chinense* QD10 cultivated with five groups of
682 carbon sources. The unique spectral biomarkers for each carbon source group are
683 labelled. Twenty infrared spectra were randomly obtained per treatment.

684 **Figure 5.** (A) Cluster vector of *S. chinense* QD10 cultivated with 48 different carbon
685 sources. Colour bars illustrate IR bands possessing significant correlations ($p < 0.05$)
686 with growth index (GI, green), Pb biosorption efficiency (blue) and Cd biosorption
687 efficiency (red). IR bands significantly correlate with GI include: (B) 1340 cm^{-1}

688 (collagen), (C) 1136 cm^{-1} (collagen) and (D) 966 cm^{-1} (C-C DNA). IR bands
689 significantly correlate with Cd biosorption efficiency include: (E) 1745 cm^{-1}
690 (phospholipids), (F) 1620 cm^{-1} (nucleic acid), (G) 1456 cm^{-1} (lipids and proteins), (H)
691 1396 cm^{-1} (proteins) and (I) 1057 cm^{-1} (stretching C-O deoxyribose).

Journal Pre-proof

(A)



(B)

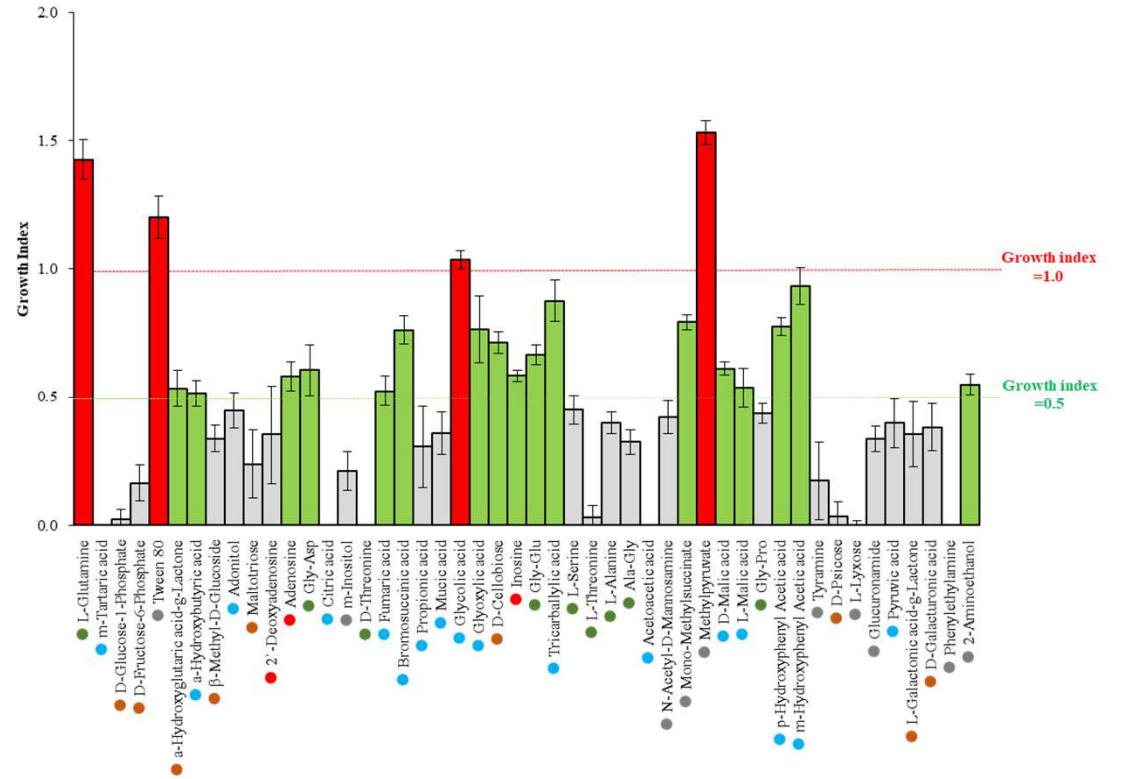


Figure 1

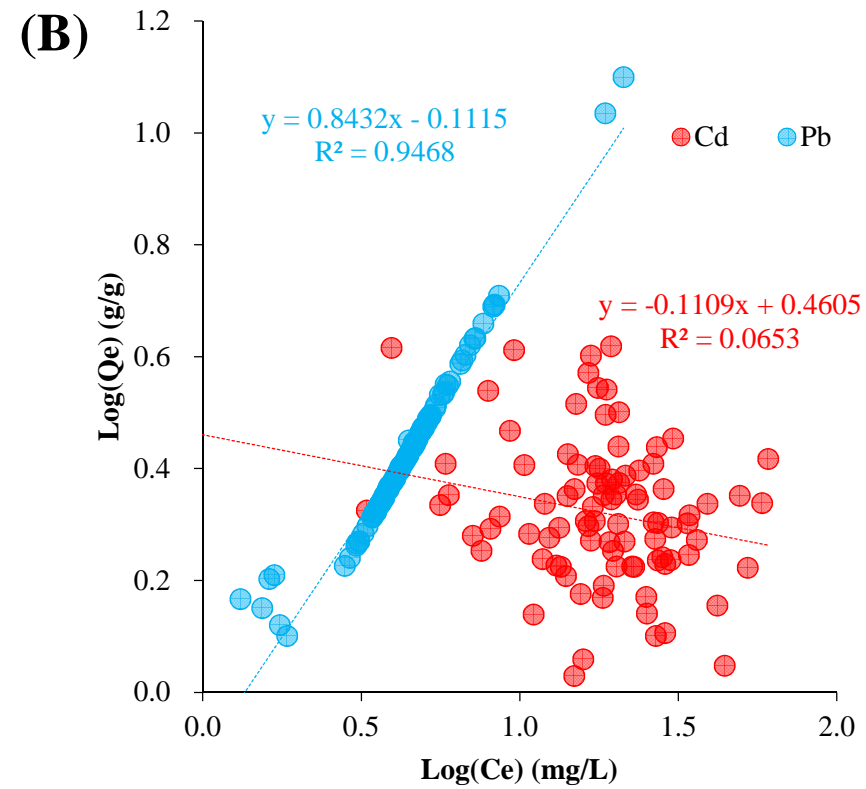
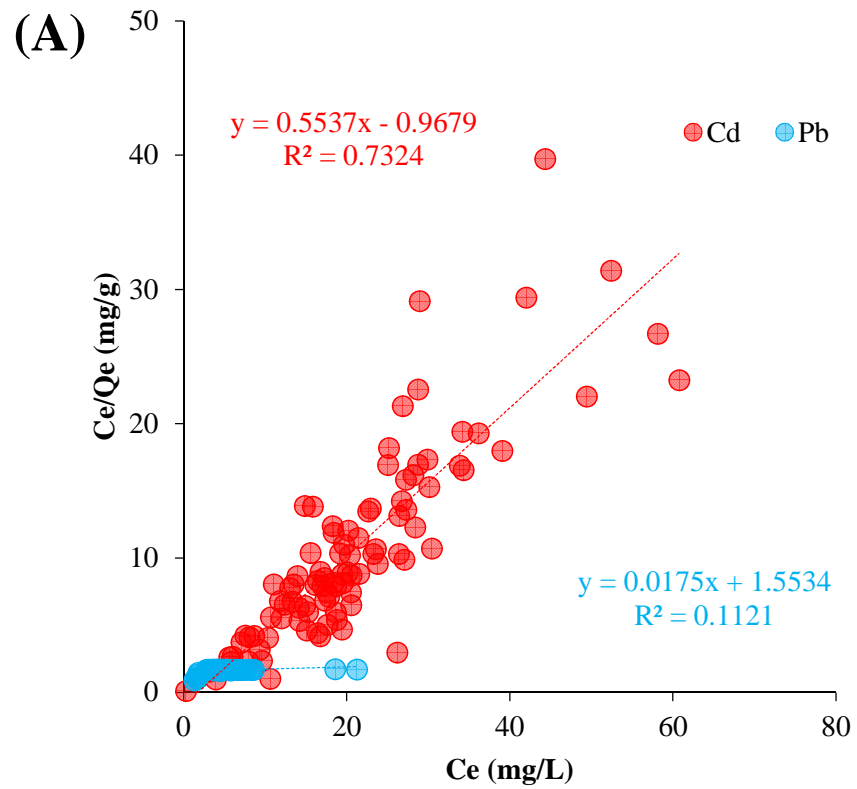


Figure 2

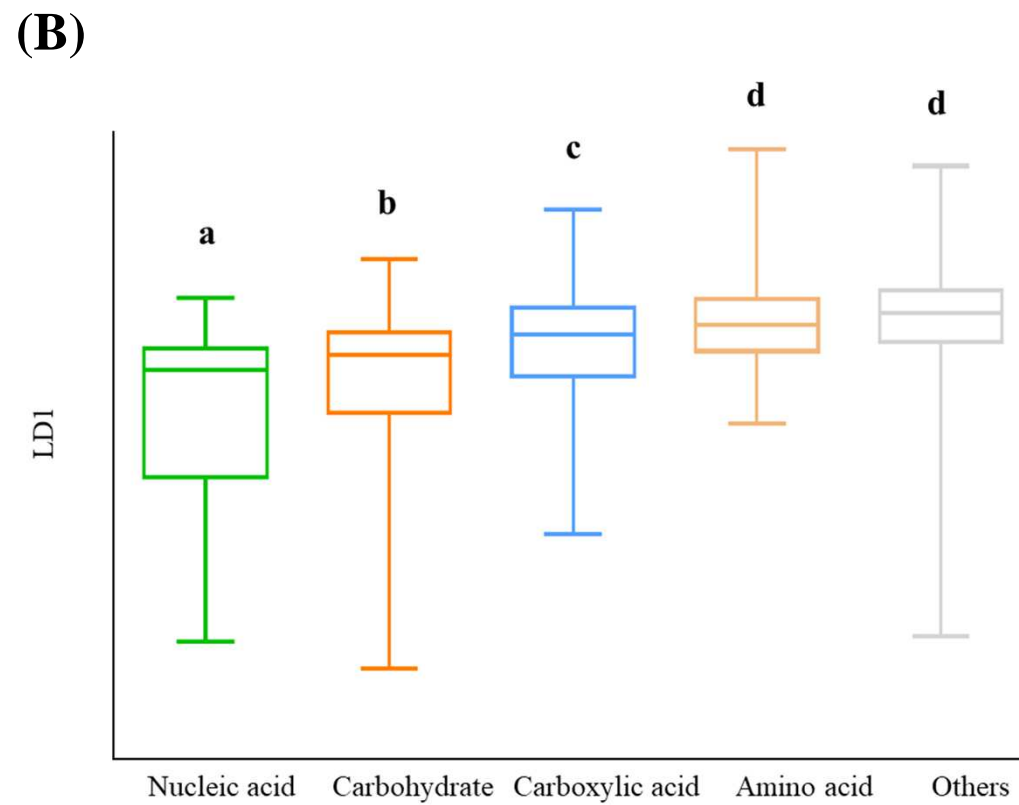
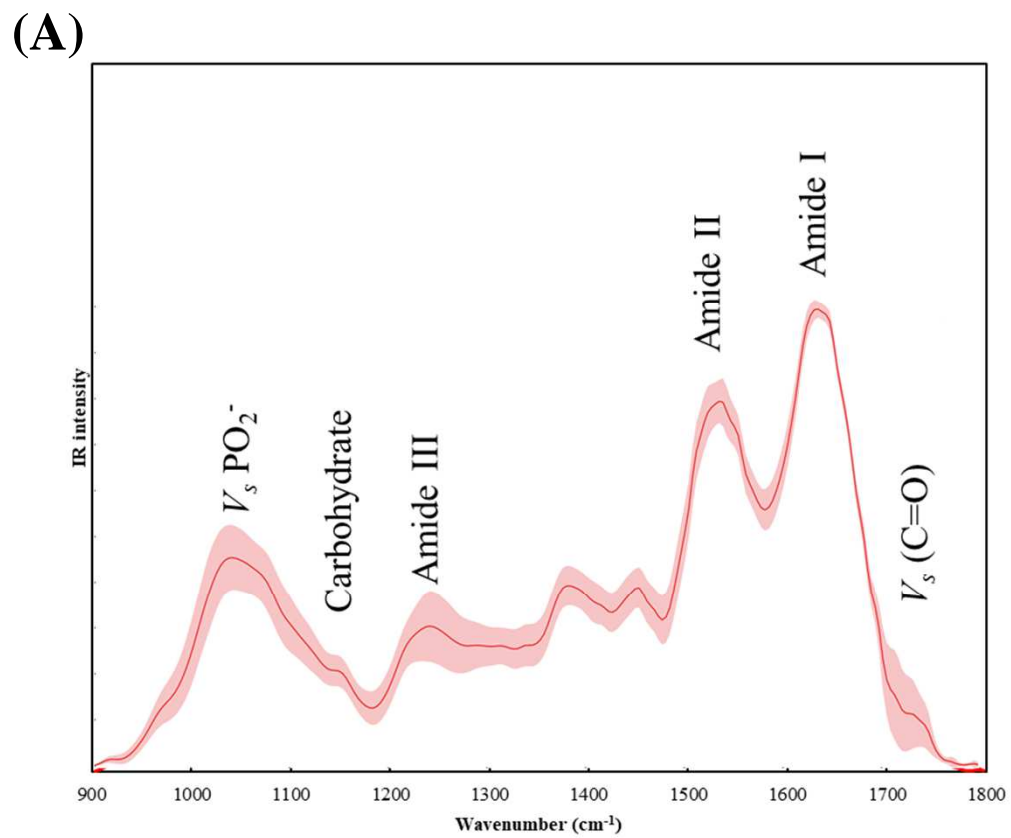


Figure 3

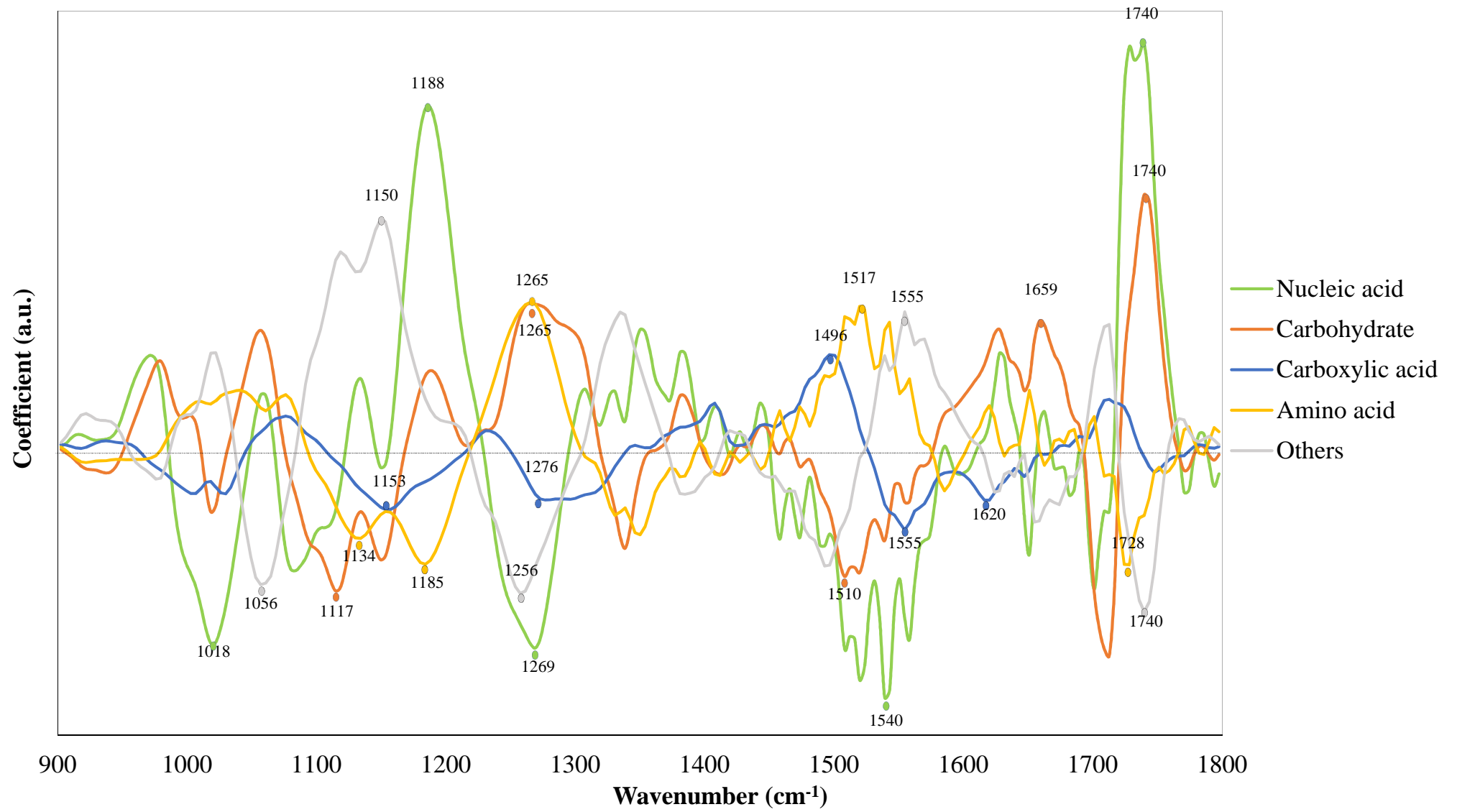
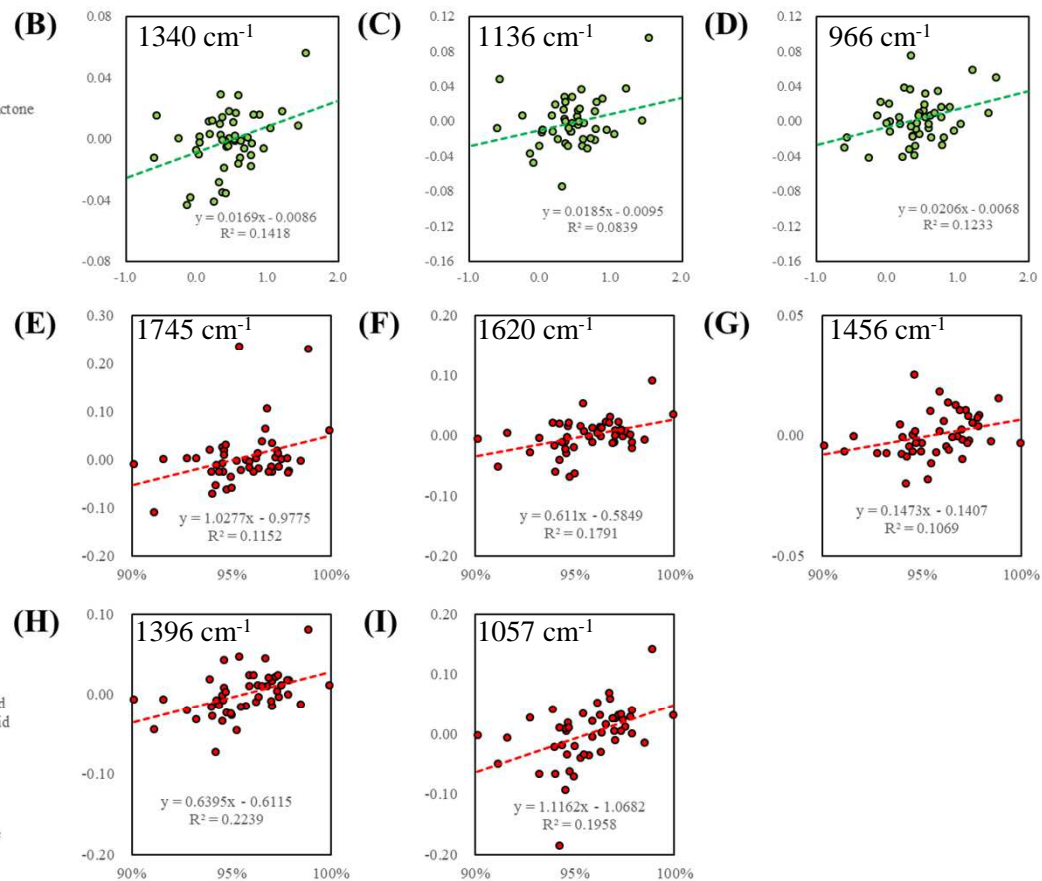
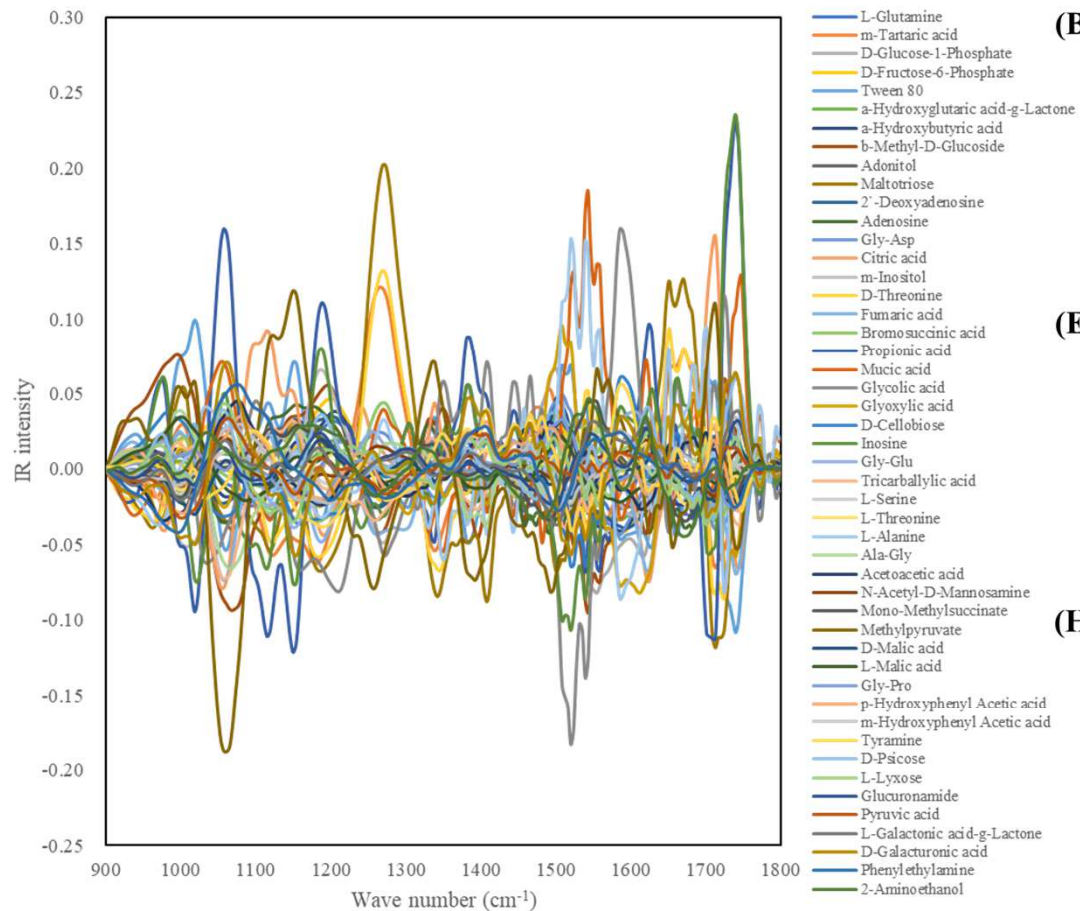


Figure 4

(A)**Figure 5**

Highlights

- 1) Cd/Pb biosorption performance by *S. chinense* QD10 across 48 carbon sources
- 2) Langmuir model for Cd biosorption and Freundlich model for Pb biosorption
- 3) First ATR-FTIR spectroscopic study on metal biosorption mechanisms
- 4) Novel spectral biomarkers for fungal growth and Cd biosorption

Journal Pre-proof

Declaration of interests

The authors declare that they have no known competing financial interests or personal relationships that could have appeared to influence the work reported in this paper.

The authors declare the following financial interests/personal relationships which may be considered as potential competing interests: